Published in "Earth and Planetary Science Letters 256(1-2): 36-46, 2007"
which should be cited to refer to this work.

Reaction-induced strain localization: Torsion experiments on dolomite

Claudio Delle Piane [a,*], Luigi Burlini [a], Bernard Grobety [b]

[a] *Geological Institute ETH, Leonhardstrasse, 19/LEB Zurich, CH-8092, Switzerland*
[b] *Department of Geosciences, University of Fribourg, Perolles, Fribourg, CH-1700, Switzerland*

Abstract

We investigated the mechanical behaviour and microstructural evolution of a dolomite marble from Mt. Frerone (Adamello, N-Italy) during decarbonation to calcite and periclase in torsion experiments. Tests were performed in a Paterson gas-medium apparatus on cylindrical samples of 10 mm diameter and 10 mm length. Experiments were conducted at 800 °C, 300 MPa confining pressure under both vented and non-vented conditions, up to a maximum bulk shear strain of about $\gamma = 1.8$, at different strain rates (3×10^{-5} s^{-1} up to 3×10^{-4} s^{-1}). Under hydrostatic conditions the nominal equilibrium $P(CO_2)$ should be around 100 MPa, but in the vented experiments the CO_2 was free to escape, causing the breakdown of dolomite.

During the decomposition, deformation was systematically localized at the ends of the specimens, near the porous spacers into a fine-grained mixture of calcite and periclase.

Due to the low permeability of the marble, pore fluid could not escape from the central part of the sample building up CO_2 pressure which suppressed the decarbonation reaction. The fluid pressure embrittled the material and caused the development of en-echelon tension fractures, inclined opposite to the sense of shear.

We conclude that decarbonation produced a weak polyphase matrix composed of submicron sized reaction products. Such a small grain size induced strain localization which was probably promoted by a switch from grain-size insensitive to grain-size sensitive deformation mechanism.

Keywords: shear zone; reaction softening; strain localization; deformation mechanism; dolomite; decarbonation

1. Introduction

Strain localization in rocks results in the formation of shear zones. These can occur over a wide range of scales from individual grains (deformation bands and kinks) to high strain zones at the crustal scale, which typically consist of planar mylonites bounded by zones that display continuous transition to the unstrained protolith (e.g. [1]).

The formation of shear zones in rocks requires the occurrence of localized strain softening leading to the loss of load-bearing capacity relative to the host rock [2]. In order to explain the loss of load-bearing capacity, a number of mechanisms have been proposed (see review [3]). Geological and experimental studies

* Corresponding author. Tel.: +41 44 632 3636; fax: +41 1 6321080.
E-mail addresses: claudio.dellepiane@erdw.ethz.ch (C. Delle Piane), burlini@erdw.ethz.ch (L. Burlini), bernard.grobety@unifr.ch (B. Grobety).

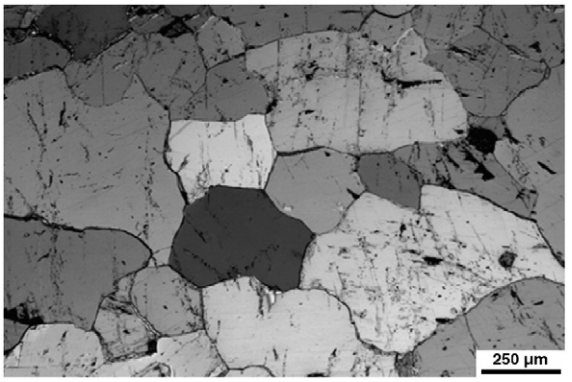

Fig. 1. Microstructure of the staring material. Cross-polarized micro-photograph showing coarse-grained dolomitic marble with straight grain boundaries, equilibrium triple junctions.

indicate that mineral reactions may have an important influence on the strength and therefore on the deformation behaviour of a rock. Overviews on possible weakening effects due to metamorphic reactions were analysed by different authors [4–8]. Many authors have shown that reactions can lead to the nucleation of fine-grained reaction products which may promote a more efficient (faster) deformation mechanism [7,9–14].

Previous experimental investigations on this topic focused on the role of water on deformation during dehydration [12,15–17] and hydration reactions [14,18]. Solid–solid syn-deformation reactions such as the transformation under anhydrous conditions of an olivine–plagioclase aggregates into an orthopyroxene+clinopyroxene+spinel assemblage have been observed to lead to weakening and strain localization [19,20].

The aim of this study is to investigate the influence of a decarbonation reaction on the deformation behaviour of polycrystalline natural dolomite during shear deformation. Torsion experiments were performed under drained conditions in the stability field of the breakdown products of dolomite i.e. calcite and periclase. Triaxial compression experiments were conducted in non-drained configuration in the stability field of dolomite in order to compare the strengths of the reacting with that of the non-reacting material. The results are compared with previous experimental studies and with natural situations to address the problem of strain localization.

2. Starting material

Metamorphosed coarse-grained dolomitic marble was sampled from the Permo–Triassic sequence of the contact aureole of the Adamello pluton (Southern Alps, Italy).

At the microscopic scale the dolomitic marble shows no or very little signs of deformation. The microstructure is characterized by very coarse grains, ranging from 100 to 700 μm in diameter, with straight grain boundaries, equilibrium triple junctions, few, widely spaced, thin and straight twin lamellae per grain, uniform extinction and no microscopic evidence of subgrains, shape or lattice preferred orientations or other deformation features (Fig. 1).

The chemical composition of the starting material, obtained from bulk X-ray Fluorescence and single-point electron microbeam analyses (Jeol JXA-8200), shows that the dolomitic marble is very pure with almost stoichiometric composition (Table 1). Microscopic investigations of thin sections revealed only occasional grains of olivine.

3. Dolomite breakdown

Dolomite decomposes according to the following reaction:

$$CaMg(CO_3)_2 \Leftrightarrow CaCO_3 + MgO + CO_2 \quad (1)$$

At constant overall pressure the equilibrium temperature of reaction (1) is only a function of the partial pressure of CO_2. Assuming the starting material is dry, the only fluid component will be CO_2 and in a closed system at 300 MPa the equilibrium temperature is 931 °C (software package PERPLE_X, [21]). The experiments under undrained conditions performed at

Table 1
Element analysis by X-ray Fluorescence on three different samples of the dolomitic marble staring material (in wt.%)

%	FRER 1	FRER 2	FRER 3	Average
SiO_2	0.43	0.28	0.73	0.48
TiO_2	0	0.01	0.01	0.01
Al_2O_3	0.19	0.19	0.28	0.22
Fe_2O_3	0.08	0.06	0.08	0.07
FeO	0	0	0	0
MnO	0	0.01	0.01	0.01
MgO	21.02	21.03	20.9	20.98
CaO	32.50	28.35	28.33	29.73
Na_2O	0.09	0.03	0.02	0.05
K_2O	0	0	0	0
P_2O_5	0	0.01	0.01	0.01
Cr_2O_3	0	0	0	0
NiO	0	0	0	0
L.O.I.	46.83	46.67	45.92	46.47
Total	101.14	96.64	96.29	98.02

Chemical formula: $Ca_{(1.009)}Mg_{(0.991)}(CO_3)_2$.
L.O.I.=loss of ignition.

800 °C were therefore within the stability field of dolomite.

Under drained conditions, the gas phase within the pores of the porous alumina spacer at the extremities of the sample is at ambient pressure and CO_2 produced during decarbonation is free to escape. The reaction creates pores, in which the fluid phase, for perfect draining conditions, will be at ambient pressure. Consequences for mineral equilibria in systems where the hydrostatic pressure is less than the lithostatic pressure have been considered by several authors (e.g. [22,23]). The thermodynamic analysis showed that the equilibria in such situations are independent of the stress state of the solid and depend only on the hydrostatic pressure of the fluid. The equilibrium breakdown temperature of dolomite grains adjacent to pores that are completely drained to ambient pressure is 430 °C. Along these interfaces the equilibrium is overstepped by 370 °C and the reaction will progress readily. Towards the interior of the sample, away from the porous spacers, the pore pressure will not be adjusted to 1 bar instantaneously. A pressure gradient and a corresponding reaction temperature overstepping gradient will be established between the reaction front and the drain. The maximum CO_2 pore pressure for which the rection will still proceed at 800 °C is 100 MPa. The speed at which the reaction front penetrates into the sample thus depends on the reaction kinetics, which dictates the evolution of the permeability.

4. Experimental procedures

4.1. Sample preparation

Specimens of 1 cm diameter were cored out of a dolomite block. Cylindrical samples of 1 cm in length and 1 cm in diameter were then cut from these cores. The planar ends of the cylindrical samples were polished down to ±5 μm. All samples were oven dried at 110 °C for at least 24 h before the experiments.

4.2. Apparatus and sample assembly

Torsion experiments were performed in an internally heated high pressure, high temperature Paterson apparatus. Argon was used as a confining pressure medium. Apparatus details and theoretical background of torsion tests on rocks are described elsewhere [14].

Before on each run, the samples are positioned between 3 mm (±0.2 mm) thick porous alumina spacers covering the solid alumina and zirconia pistons which limit conductive heat losses and guarantee a stable thermal profile along the sample length. The assembly is inserted into a 0.25 mm wall thickness, 15 mm diameter iron jacket, in order to separate the sample from the confining pressure medium. The diameter of the jacket had to be swaged in the part of the assembly corresponding to the sample+alumina spacer length in which the diameter is 10 mm. This resulted in a local thickening of the jacket itself up to a maximum thickness of 0.4 mm.

In order to visualize possible slip at the different parts of the assembly, straight reference scratches were drawn on the surface of the iron jacket parallel to the axis of the assembly.

Temperature during the experiments was monitored using a K-type thermocouple placed at about 3 mm from the top of the samples. Temperature differences across the sample obtained from regular calibration never exceeded 2 °C.

4.3. Experiments

A technical difficulty was to prevent slip at the specimen–piston interfaces under non-vented conditions. Torsion tests in such a configuration systematically resulted in some slip at one of the interfaces between the different piston in the column assembly because the shear strength of dolomite at equilibrium is higher than the friction between the parts of the assembly (164 MPa for the steel against ceramic parts

Table 2
Experimental conditions and specimen dimension for the performed experiments

Test details: Torsion (drained)

Sample #	Diameter (mm)	Length (mm)	T (°C)	Confining pressure (MPa)	Shear strain (bulk)	Shear strain rate (s^{-1})	Peak torque (N m)
FRD01	9.9	9.952	800	300	1.3	Up to 3E−4	28.96
FRD10	9.87	10.94	800	300	0.35	3E−5	17.7
FRD11	9.88	9.742	800	300	1.1	9E−5	19.64
FRD12	9.85	8.996	800	300	1	1E−4	22.76
FRD19	9.85	9.977	800	300	0.85	Up to 1E−4	24.48
FRD20	9.85	9.7	800	300	1.8	Up to 3E−4	28.54

Test details: Triaxial compression (undrained)

Sample #	Diameter (mm)	Length (mm)	T (°C)	Confining pressure (MPa)	Strain %	Strain rate (s^{-1})
FRD17	9.85	10.067	800	300	~10	7.5E−5

of the column at 300 MPa confining pressure). Therefore for non-vented conditions, the torsion experiments were replaced by triaxial compression tests using the same temperature, confining pressure and strain rate as for the torsion experiments.

Samples were shortened at nearly constant axial strain rates. Strain and strain rates were determined from measurements of axial displacement normalized to the original length of the specimen. Axial loads during triaxial compression were measured with a capacitance internal load cell, the measured values were corrected taking into account the jacket strength, the rig distortion, the change in section size of the sample during deformation and then converted into differential stress.

The resulting differential stress was converted into shear stress [14]. Sealing of the system is ensured by using solid, 3 mm thick alumina spacers to sandwich the samples.

Torsion experiments under drained conditions were run at 800 °C, 300 MPa confining pressure and shear strain rates between 3×10^{-5} s^{-1} and 3×10^{-4} s^{-1} up to different amounts of finite shear strain (Table 2). Alumina spacers with an open porosity of 20–30% were placed between the sample and the hollow ceramic pistons, so that the fluid generated by the decarbonation reaction could escape to the atmosphere. Strain rate stepping [24–26] was performed in experiments PO571, PO667 and PO678 in order to evaluate the stress exponent and therefore establish the dominant deformation mechanism at different finite shear strains, at the beginning of flow, at the end of weakening and at mechanical steady state respectively.

Torque data were corrected for jacket strength and shear stress τ was then computed using equation:

$$\tau = \frac{\left(3+\frac{1}{n}\right)M}{2\pi R^3} \quad (2)$$

Where, n is the stress exponent, M is the measured torque and R is the radius of the specimen.

4.4. Microstructural analysis techniques

Thin slabs parallel to the cylinder axis were cut close to the outer rim of the deformed specimens (longitudinal tangential [24]). Ultra-thin (<10 μm) sections were prepared from these thin slabs and studied by optical microscopy. The cut surface of the remainder of the specimen was fine polished down to 1/4 μm using diamond paste, carbon coated and examined with a CamScan CS-44 Scanning Electron Microscope (SEM). Conditions for back scattered electron (BSE) and secondary electrons (SE) imaging were: 15 kV acceleration voltage, 35 to 14 mm working distance and ~3 nA beam current. Quantitative image analyses were performed on both thin section photographs and BSE images using an image analysis software (UTHSCSA Image Tool).

X-ray diffraction (Philips, PW18000, 40 kV acceleration voltage, 40 mA tube current; step scan mode, 0.02°/step, 2 s/step) was performed on a sample surface in contact with the porous alumina end disc surface to establish the nature of the newly formed products.

5. Results

5.1. Mechanical data

5.1.1. Undrained experiments

Constant strain rate triaxial compression experiments were performed at 300 MPa confining pressure, 800 °C and strain rate of 7.5×10^{-5} s^{-1} up to an axial strain of 10%.

Under these conditions only grains adjacent to pores not filled by CO_2 will react. Considering the very small porosity of the samples, an infinitesimally small reaction increment will immediately saturate the pores with CO_2 and push the sample back into the stability field of dolomite. Thus the experimental conditions demonstrate the behaviour of dolomite with no reaction.

The stress versus axial shortening plot shows that dolomite yields at a differential stress of ca. 350 MPa and hardens until an apparent flow stress value of 500 MPa at approximately 10% shortening.

Our results fit well with those obtained in previous experimental investigation on natural dolomite marble deformed at similar conditions [27] (Fig. 2).

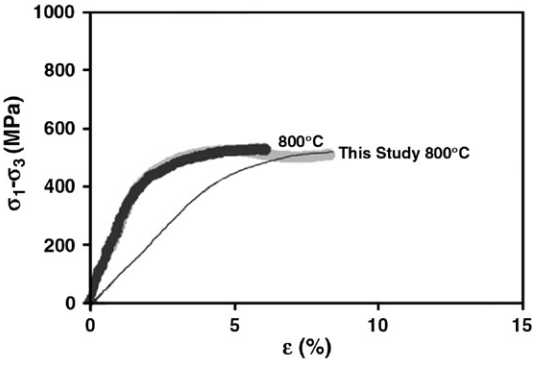

Fig. 2. Differential stress as a function of axial strain, plotted for experimentally deformed dolomite in undrained conditions. Thick lines represent data from Davis [27]. Deformation conditions are: temperature 800 °C, confining pressure 300 MPa axial strain rate is 1.25×10^{-5} s^{-1} for the experiments of Davis, and 7.5×10^{-5} s^{-1} for this study.

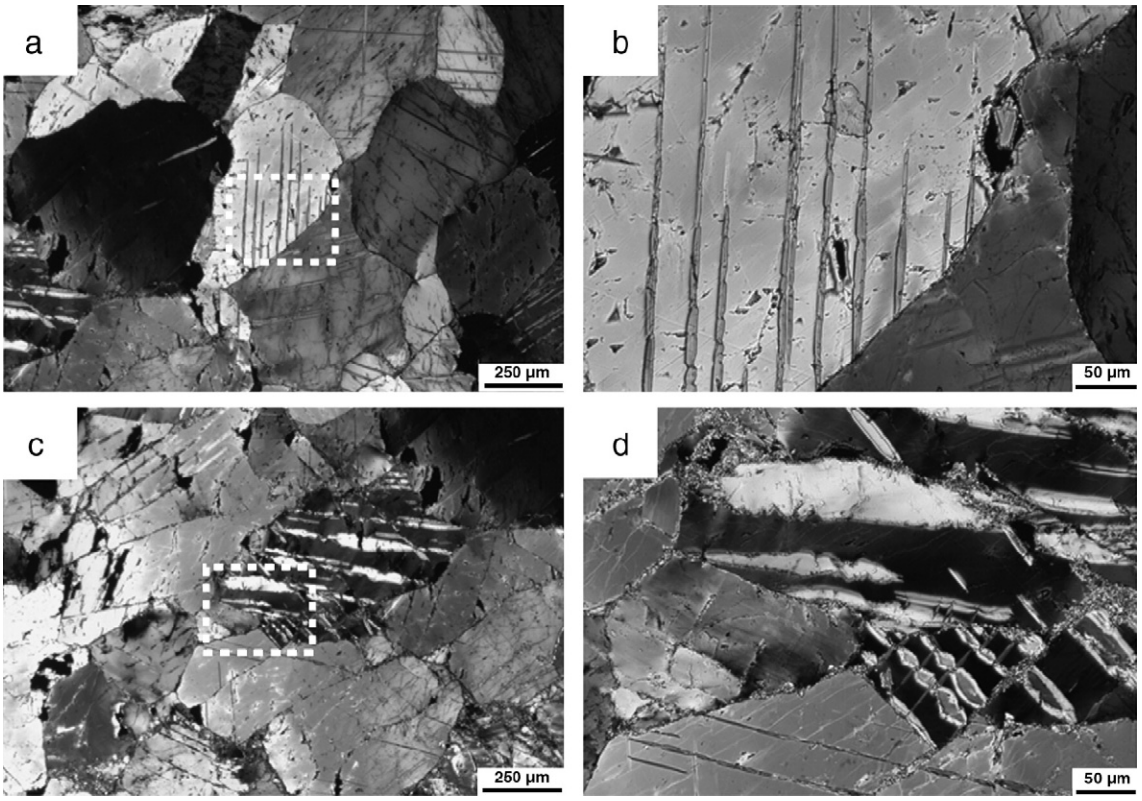

Fig. 3. Thin section photographs in cross-polarized transmitted light of samples deformed in undrained conditions. Shortening direction is vertical. (a+b) Coarse-grained dolomite with tapered edge twins and undulose extinction. (c+d) Coarse-grained dolomite showing migrated twin boundaries. Note the fine dynamically recrystallized grains decorating the grain boundaries.

5.1.2. Drained experiments

The shear stress–bulk shear strain curves obtained in the various experiments (Fig. 4) show similar patterns with a very fast transition from primary creep to weakening regime at very low values of shear strain ($\gamma = 0.06 \pm 0.02$). After a post-yield weakening of ~30% with respect to the peak torque the material continues to deform under constant torsional load. Experiments usually ended with jacket failure.

The value of peak torque increases with increasing strain rates, ranging between 18 N m at 3×10^{-5} s^{-1} and 29 N m at 3×10^{-4} s^{-1} at the outer surface of the specimen.

In order to establish the strain rate sensitivity of the strength of the material, shear strain rate stepping was performed at different finite shear strains. At low strain, when the material is still in the primary creep regime, an apparent strain rate sensitivity of 6 was obtained while for higher strains, when deformation proceeds under constant torque, the strain rate sensitivity yields a value of 1.9. Thus, the *n*-value decreases for increasing strain, which suggests a more important effect of diffusion creep on the overall deformation process and that different deformation mechanisms are dominant for different finite strains.

5.2. Microstructures and phase identification

5.2.1. Undrained experiments

Under light microscope examination, samples deformed at 800 °C have a microstructure compatible with intracrystalline plasticity. Twin density exceeds that of the starting material and twins often show tapering edges or evidence for twin boundary migration. Individual coarse grains of dolomite show undulose extinction and grain boundaries are decorated by fine recrystallized grains. Dynamically recrystallized grains are also visible within coarse grains along twin traces or cracks (Fig. 3).

5.2.2. Drained experiments

The straight, vertical scratches marked on the iron jacket before the torsion experiments became only slightly inclined in the central part of the sample, whereas they are strongly inclined in two narrow zones adjacent to the top and bottom ends of the specimens (Fig. 5). These zones correspond to ~0.3 mm thick layers of ultra-fine-grained material whose grain size is not resolvable under optical microscopy (Fig. 6). This fine-grained matrix has a foliation making an angle of 5 to 10° with the interfaces

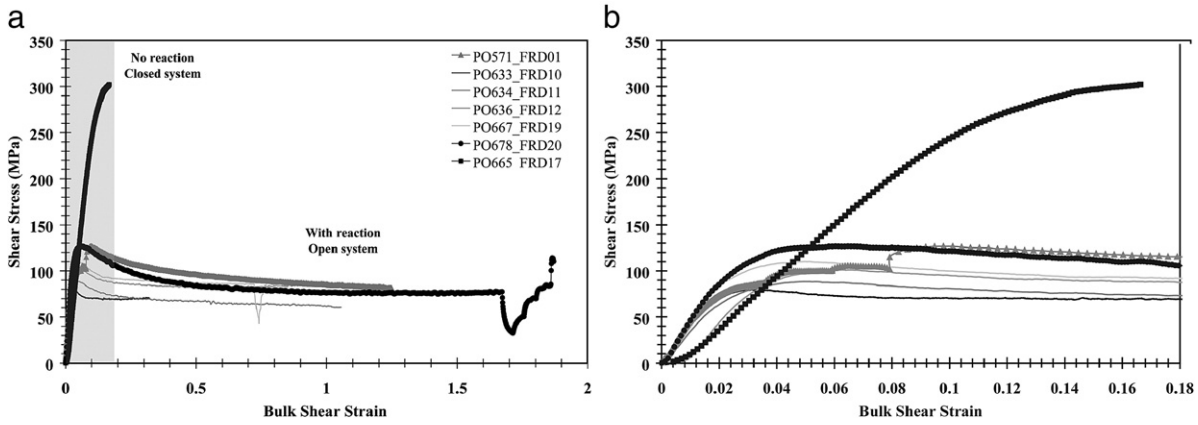

Fig. 4. (a) Shear stress as a function of bulk shear strain for the performed experiments. The data for experiment PO665 represent differential stress converted into shear stress (see text for details). Strain rate stepping was performed in experiments PO571, PO667 and PO678 at the beginning of flow, at the end of weakening and at the mechanical steady state respectively. (b) Blow up of the shaded area of a.

between sample and spacers; the acute angle points to the direction of the imposed sense of shear (Fig. 6). The grain size observed in secondary electron images (SE) ranges between 1/4 and 1 μm (Fig. 7).

Moving away from the sample–spacer interfaces the fine-grained material becomes less abundant and the inclination of the foliation becomes steeper. Coarse non-reacted grains of dolomite are present showing evidence of internal deformation like undulose extinction, micro cracks, as well as displaced and bent twin boundaries. The grain boundaries are decorated with ultra-fine material which is also present along twins and cracks.

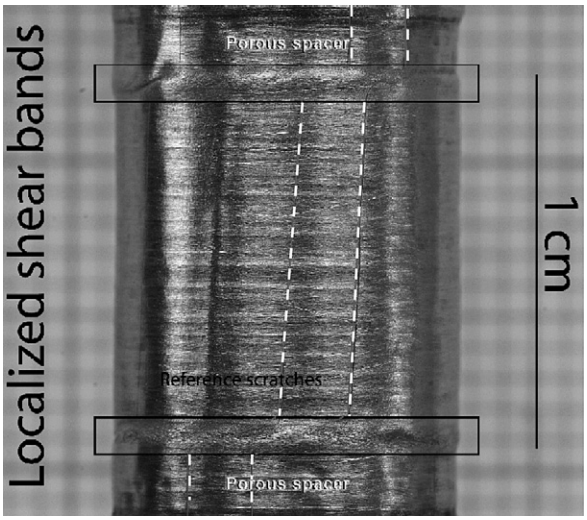

Fig. 5. Photograph of a deformed sample still inserted in the iron jacket. Reference scratches were initially parallel to the cylinder axis and serve as passive strain markers to illustrate simple shear deformation. Note the difference in inclination of the scratches at the top and bottom sample–spacers interfaces and in the central part of the specimen. Sense of shear is top-to-right.

The contrast in the BSE images, and the results from EDS and XRD analyses reveal that the fine-grained material is composed of a mixture of calcite and periclase, with few non-reacted, deformed dolomite clasts. These grains have an average aspect ratio of 2:1 and show a shape preferred orientation with the long axis forming an angle of ~14° with respect to the sample–spacer interfaces. The weight fraction of both product phases obtained from Rietveld refinement of the XRD patterns corresponds to the stoichiometry of reaction (1). No brucite was detected.

Tension fractures developed across the central zone of the samples oriented at ca. 45° with respect of the samples ends, an orientation consistent with direction of the principal stresses induced by the applied torsion (Fig. 8d).

High magnification SEM images of the reacted zones reveal very small porosity, of the order of 1–5%.

6. Discussion

6.1. Deformation mechanisms

Microstructural observations showed evidence for different deformation mechanisms to be active in different regions of the samples deformed under vented conditions (Fig. 8). The occurrence of twin bands and migrated twin boundaries in the coarse, non-reacted dolomitic grains in the specimen centre is reminiscent of intracrystalline plastic deformation, which however is only able to account for very limited amount of strain; the inclination of the reference scratches on the jackets in the central part of the deformed specimens indicates a shear strain between 0.03 and 0.09.

In the shear zones at both ends of the sample, grains of calcite and periclase with equivalent diameter as small as 0.25 μm are present. According

to [28], for calcite grains smaller than 10 μm and under experimental conditions applied in this study, the deformation mechanism is expected to become grain size sensitive. The beginning of the weakening regime coincides probably with the moment in which zones with fine-grained reaction products become interconnected and the deformation is dominated by grain size sensitive processes. The stress exponent value revealed by strain rate stepping tests in the weakening and steady state regimes is higher than the purely linear viscous behaviour expected for diffusion creep deformation regime. Assuming the ultra-fine grain aggregate deforms by grain-boundary sliding, different accommodation processes may explain variations in the stress exponent: n is expected to be 1 for purely diffusional accommodation and 2 for accommodation by processes involving grain-boundary and intragranular dislocation motion [28].

Tension fractures indicate brittle failure. They normally formed in the central part of the specimens where, due to the low permeability of the starting material, dolomite is stable (Fig. 8d). The orientation of these fractures remains in agreement with the geometry of the principal stress directions induced by the applied torsion, with the σ_1 oblique to the sense of shear. CO_2 production due to the equilibrium reaction of dolomite might lead to the formation of fluid pressure which would locally lower the effective pressure and thus favour cataclastic deformation. Microstructural analysis of these fractures shows no displacement along their planes, probably meaning that these discontinuities are formed in the latest deformation phase. BSE images reveal no chemical variation along the fracture planes, suggesting that even after brittle failure fluids were under a pressure high enough to keep dolomite stable. Thus the fracturing did not change the drainage of the samples. No stress drop attributable to brittle failure was measured during the experiments.

6.2. Strain partitioning

We estimated the difference in strain and strain rate between the shear zone and the non-reacted dolomitic core of the sample, using two different approaches. As an example we report the results obtained from the analysis of sample FRD10.

1. using UTHSCSA Image Tool software we measured the angles of the foliation in the shear zones with respect to the sample–porous spacer interface (representing the shear zone boundary) and used these values to calculate the corresponding shear strain by using the relationship between the angular shear (ψ) and the shear strain (γ):

$$\gamma = \tan\psi. \tag{3}$$

   The same procedure was followed to calculate the shear strain in the central part of the samples, but using the inclination of the reference scratches on the iron jacket instead of the sample foliation. The mean shear strain was 11 for the shear zones and 0.07 for the core of the samples; and the corresponding shear strain rates are 9.71×10^{-4} s^{-1} of 5.85×10^{-6} s^{-1}.

2. since the sum of the host rock and shear zones strain rates times their respective volume fractions must equal the bulk shear strain rate [17], the known values of bulk strain rate, shear strain, strain rate and volume fraction of the "host rock" may be used to recalculate the shear strain and strain rate in the shear zones. The values obtained by this method, 10.8 and 9.25×10^{-4} s^{-1} for strain and strain rate respectively, are in very good agreement with those obtained with the previous approach.

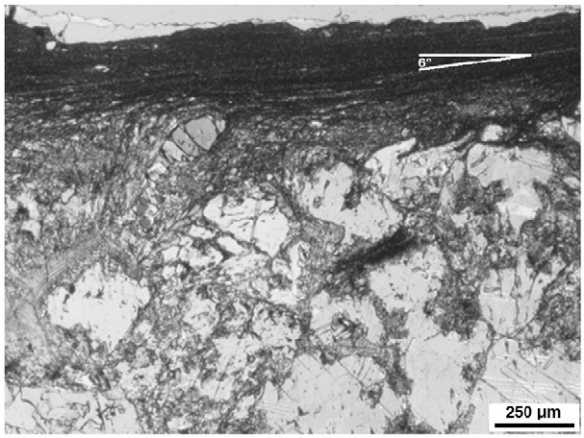

Fig. 6. Thin section photographs in cross-polarized transmitted light of the top part of deformed sample FRD11; tangential cut. White lines highlight the foliation in the fine-grained aggregate, and its angle with respect of the shear zone boundary. Sense of shear is top-to-right.

The difference in shear strain of two orders of magnitude between the shear zones and the non-reacted core is typical for all samples. A switch from deformation based on crystal plasticity in the coarse original dolomitic grains, to grain size sensitive mechanisms operating in the fine-grained reaction products, may explain the strain partitioning between different portions of the sample.

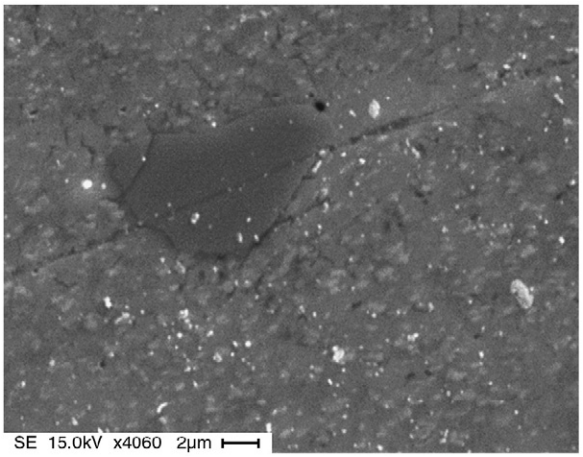

Fig. 7. SEM image in secondary electron mode of deformed sample FRD20. The image is taken in the fine-grained reaction products shear zone in the top part of the sample. The dark grey clast is dolomite, surrounded by ultra-fine calcite and periclase. Note the very small residual porosity. Shear sense is top-to-right.

6.3. Reaction softening

To initiate and maintain a high strain zone it is necessary for the rock strength in the shear zone to be less than that of the host rock (e.g. [29]). Several experimental studies demonstrated that grain size refinement can be associated with strain weakening. A number of processes might lead to grain size reduction: dynamic recrystallization is thought to cause softening by replacing strained crystals with dislocation free grains [30–32]. A change in deformation mechanism from dislocation creep to grain size sensitive flow has been suggested to follow grain size reduction by recrystallization [33,34]. On the other hand it has been argued [35,36] that syn-deformation grain growth would slow deformation in the grain size sensitive deformation regime until grain sizes were large enough for deformation by dislocation creep to be more efficient, which in turn would lead to grain refinement by recrystallization. The competition between these two processes would prevent significant strain softening. The authors [35,36] also specify that significant weakening by grain size reduction in localized shear zones may be possible only if caused by processes other than dynamic recrystallization such as syntectonic reactions and if grain growth is inhibited.

In our experiments nucleation of new phases during decarbonation reaction of dolomite is an extremely efficient mechanism for grain size reduction as newly formed calcite and periclase show submicron size. In order to maintain the rock weakened after grain size reduction, the preservation of small grains is essential.

The mobility of grain boundaries during growth is strongly affected by the presence of a solid second phase. In the case of polymineralic aggregates with a volumetrically dominant matrix phase and homogeneously dispersed second phases, the matrix grains will undergo normal grain growth until their grain boundaries become immobile because of a process called Zener pinning [37–39]. Phase boundary pinning is optimised in well-mixed polyphase materials, and XRD analysis on our deformed samples showed that the decarbonation reaction of dolomite produced a polyphase aggregate with a molar distribution of 1:1 between Cc and Per. This corresponds to a volume ratio calcite:periclase of ca. 3 to 1, calcite is thus the matrix phase and periclase the dispersed second phase, such a distribution appears to be very effective in suppressing grain growth over the duration of an experiment.

We calculated the theoretical values of volume reduction due to the decarbonation reaction using Perplex and published thermodynamical data base [40]. Because the solid volume of calcite and periclase is ca. 25% smaller than that of dolomite, the decarbonation reaction will at least transiently produce porosity. Through SEM imaging we estimated a residual porosity of 1–5% in the deformed samples; therefore porosity, once produced, was destroyed by plastic creep and pore collapse due to high effective pressure until when the permeability was high enough to let the CO_2 escape. Such a solid volume reduction is likely to have an influence on the strength of the deforming material both at the sample scale and at the grain scale. A solid volume replaced by a void (pore) leads to stress concentration in the reacted products. This in turn may enhance deformation and eventually lead to weakening.

6.4. Dislocation creep vs. diffusion creep

The very small grain size of the reaction products and the stress exponent value of 1.9 from the stepping rate test at high strain suggest activity of a grain size sensitive deformation mechanism inside the shear zones. To test this hypothesis we used the published flow law for calcite to calculate what the predicted shear stress would be in our experiments. We compared the results using the flow law from [41] for the grain size insensitive (GSI) creep, and from [28] for the grain size sensitive (GSS) creep. The initial input for both laws is the shear strain rate in the shear zone of our experiments as it is estimated from optical analysis (see above for details). We used a representative value of 9.7×10^{-4} s^{-1} for the local shear strain rate. The grain size (0.25 μm) used for the GSS case is inferred from SEM images.

The results of the calculations are summarised in Table 3. If we consider the shear zone to be composed of

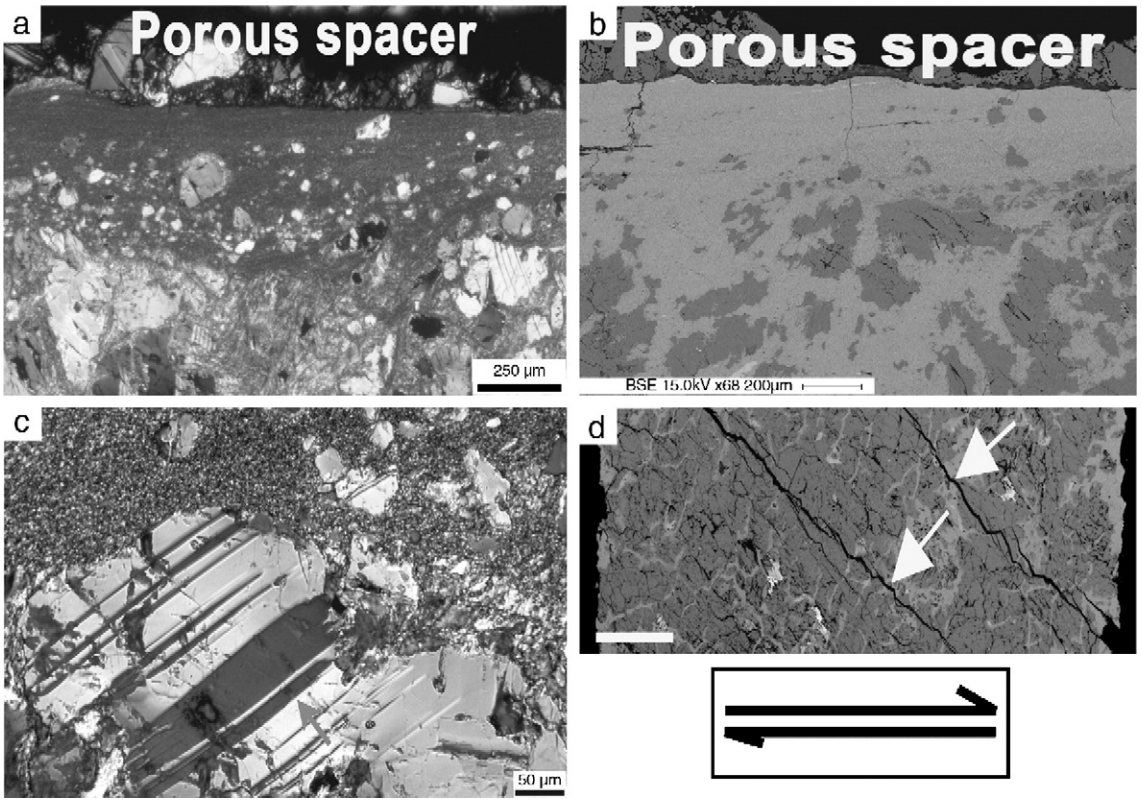

Fig. 8. Mosaic showing microstructures derived from activity of different deformation mechanisms. (a) Thin section photographs in cross-polarized transmitted light of the top part of deformed sample, the shear zone is deforming through grain size sensitive creep. (b) SEM image in back scattered electrons mode of the top part of the deformed sample. Note the different grey level (corresponding to different chemical composition) between the shear zone and the dark grey dolomitic clasts. (c) Thin section photographs in cross-polarized transmitted light showing intracrystalline deformation (twins and twin boundary migration) of a clast of dolomite surrounded by fine-grained reaction products. (d) Back scattered electron image of the central part of deformed sample FRD01. The composition is rather homogeneous, due to the high CO_2 pressure which stabilizes the dolomite. Brittle fractures (indicated by white arrows) are crossing the sample. White scale bar is 1 mm. Sense of shear is top-to-right in all images.

pure calcite we obtain unrealistically low values of shear stress in the GSS case, while for the dislocation creep assumption we obtain values of the same order of magnitude as the measured ones, i.e. 70–90 MPa (Fig. 4). As shown before, XRD analysis suggests that the shear zone should be considered as constituted of a calcite matrix with dispersed periclase in it, with a volume ratio calcite:periclase = 3:1. This implies that periclase might have a strong influence on the bulk strength of the shear zone.

Table 3
Flow laws parameters used for the calculations of the shear stress of calcite in the GSI creep, and GSS creep

	Flow law GSI creep	Flow law GSS creep	
	$\varepsilon = A\ \exp(-Q/RT)\sigma^n$	$\varepsilon = A\ \exp(-Q/RT)\sigma^n d^m$	
A	1258	79432	
Q	418000	190000	J/mol
n	7.6	1.7	
R	8.314	8.314	J/(mol K)
T	1073	1073	K
τ	**40.11**	**0.54**	MPa
γ	9.7E−04	9.7E−04	s^{-1}
d	-	0.25	µm
m	-	−1.9	

The calculated shear stress is highlighted in bold.

Published experimental work on polycrystalline MgO revealed that periclase is stronger than calcite and yields at a shear stress of ca. 160 MPa [42] at conditions similar to those of our experiments.

We can thus assume the shear zone to be a bimineralic aggregate composed of a weak and a strong phase. An upper bound to the calculated strength of such material is given by:

$$\tau = \tau_w \phi_w + \tau_s \phi_s$$

where τ is the shear strength, ϕ is the volume proportion of the phase, the subscript "w" or "s", stands for weak or strong phase [43].

The shear strength attains a value of 49 MPa and 77 MPa for GSS and GSI creep respectively. In conclusion the flow law that best approaches our result is the one for grain size insensitive creep, even though the stress exponent has a value of 1.9 in our experiments and the submicron size of the grains would favour diffusion creep.

This mismatch might be due to an underestimation of the shear strain rate in the shear zone; on the images used for our estimation the geometry of microstructures is often ambiguous due to the very fine-grain size. More over it is difficult to trace a limit and establish the thickness and volume of the shear zone.

Assuming that our estimates are good, then the flow law we used is inappropriate to describe large strain deformation processes for such fine-grained aggregate. Moreover none of the available flow laws accounts for enhanced ductility due to syn-reaction solid volume reduction and pore collapse.

7. Conclusions

We deformed cylindrical samples of a natural dolomitic marble in torsion experiments under drained conditions at temperature causing the following decarbonation reaction:

$$CaMg(CO_3)_2 \Leftrightarrow CaCO_3 + MgO + CO_2.$$

Reaction progress is controlled by the CO_2 pressure gradient along the sample which is in turn controlled by the permeability of the specimens. Fine-grained (sub micron size) products of the reaction are found at the interface between the sample and the porous spacers where CO_2 was free to escape, forming a layer of approximately 200 μm. The presence of such a small grain size promotes the activation of grain size sensitive deformation mechanism and strain and strain rate partitioning into the reaction products layers. In these zones the final strain is two orders of magnitudes higher than in the core, non-reacted part of the sample which shows evidence for intracrystalline deformation. Thus the weakening is associated with grain size refinement due to the decarbonation reaction, which induces a switch from grain-size insensitive deformation mechanism in the coarse non-reacted dolomitic grains, into grain-size sensitive creep in the polyphase reaction products. The maintenance of the localization into (two) shear zones was ensured by pinning between different phases which suppressed grain growth and kept a very fine-grain size which promoted the grain-size sensitive creep.

The strength of reacting dolomite is compared with that of dolomite deformed in triaxial compression in non-drained conditions, which appears to be much stronger. The bulk rheology of dolomite deformed in drained conditions is therefore controlled by strength of the reaction products.

Examples of natural shear zones highlight the importance of reaction softening as a major mechanism for strain localization at different levels of the Earth from the upper mantle to the surface.

Acknowledgements

This work is part of the PhD project of Claudio Delle Piane, ETH grant TH 1/03-3/2704.5. Laboratory equipment and analyses were supported by the NF grant 01066/41-2704.5 and the ETH grant # 02150/41-2704.5. R. Hofmann and M. Metzler are thanked for the technical support in the laboratory and for the maintenance of the apparatus; F. Pirovino is thanked for the thin section preparation, U. Gerber for help with microphotos.

M. Bystricky and T. Hirose are thanked for helpful discussions in the laboratory. K. Kunze is thanked for help with the SEM work. A. Delacour and P. Ulmer provided assistance for the XRF analyses, L. Caricchi for the microprobe analyses. P. Brack and J.-P. Burg are thanked for the support in the field and for stimulating discussions.

J. Connolly is thanked for the fast Perplex calculation.

Constructive reviews from E. Rutter and I. Jackson have substantially improved the final version of the manuscript.

References

[1] J.C. Ramsay, Shear zone geometry: a review, J. Struct. Geol. 2 (1980) 83–99.

[2] B.E. Hobbs, H.B. Muhlhaus, A. Ord, Instability softening and localization of deformation, in: R.J. Knipe, E.H. Rutter (Eds.), Deformation Mechanism, Rheology and Tectonics: Geological Society, London, Special Publications, vol. 54, 1990, pp. 143–165.

[3] L. Burlini, D. Bruhn, High strain zones: laboratory perspectives on strain softening during ductile deformation, in: D. Bruhn, L. Burlini (Eds.), High-Strain Zones: Structure and Physical Properties: Geological Society of London, Special Publications, vol. 245, 2005, pp. 1–24.

[4] S.H. White, S.E. Burrows, J. Carreras, N.D. Shaw, F.J. Humphreys, On mylonites in ductile shear zones, J. Struct. Geol. 2 (1980).

[5] K.H. Brodie, E.H. Rutter, On the relationship between deformation and metamorphism, with special reference to the behaviour of basic rocks, in: A.B. Thompson, D.C. Rubie (Eds.),

Metamorphic Reactions: Kinetics, Textures and Deformation, Springer-Verlag, New York, 1985, pp. 138–179.
[6] K.H. Brodie, E.H. Rutter, The role of transiently fine-grained reaction products in syntectonic metamorphism natural and experimental examples, Can. J. Earth Sci. 24 (1987) 556–564.
[7] D.C. Rubie, Mechanisms of reaction-enhanced deformability in minerals and rocks, in: D.J. Barber, P.G. Meredith (Eds.), Deformation Processes in Minerals, Ceramics and Rocks, Unwin Hyman, London, 1990, pp. 262–295.
[8] E.H. Rutter, K.H. Brodie, Mechanistic interactions between deformation and metamorphism, Geol. J. 30 (1995) 227–240.
[9] A.M. Boullier, Y. Gueguen, SP-mylonites: origin of some mylonites by superplastic flow, Contrib. Mineral. Petrol. 50 (1975) 93–104.
[10] R. Kerrich, I. Allison, R.L. Barnett, S. Moss, J. Starkey, Microstructural and chemical transformations accompanying deformation of granite in a shear zone at Mieville, Switzerland; with implications for stress corrosion cracking and superplastic flow, Contrib. Mineral. Petrol. 73 (1980) 221.
[11] D.C. Rubie, Reaction enhanced ductility: the role of solid–solid uni-variant reaction in deformation of the crust and mantle, Tectonophysics 96 (1983) 331–352.
[12] E.H. Rutter, K.H. Brodie, Experimental "syntectonic" dehydration of serpentinite under conditions of controlled pore water pressure, J. Geophys. Res. 93 (1988) 4907–4932.
[13] J. Newman, W. Lamb, M. Drury, R. Vissers, Deformation processes in a peridotite shear zone: reaction softening by an H_2O-deficient, continuous net transfer reaction, Tectonophysics 303 (1999) 193–222.
[14] H. Stunitz, J. Tullis, Weakening and strain localization produced by syn-deformational reaction of plagioclase, Int. J. Earth Sci. 90 (2001) 136.
[15] S.A.F. Murrel, I.A.H. Ismail, The effect of decomposition of hydrous minerals on the mechanical properties of rocks at high pressures and temperatures, Tectonophysics 31 (1976) 207–235.
[16] D.L. Olgaard, S.-c. Ko, T.-f. Wong, Deformation and pore pressure in dehydrating gypsum under transiently drained conditions, Tectonophysics 245 (1995) 237.
[17] I. Caleb, W. Holyoke, J. Tullis, Formation and maintenance of shear zones, Geology 34 (2006) 105–108.
[18] E.H. Rutter, C.J. Peach, S.H. White, D. Johnston, Experimental "syntectonic" hydration of basalt, J. Struct. Geol. 7 (1985) 251.
[19] A.A. De Ronde, R. Heilbronner, H. Stunitz, J. Tullis, Spatial distribution of deformation and mineral reaction in experimentally deformed plagioclase–olivine aggregates, Tectonophysics 389 (2004) 93–109.
[20] A.A. De Ronde, H. Stunitz, J. Tullis, R. Heilbronner, Reaction-induced weakening of plagioclase–olivine composites, Tectonophysics 409 (2005) 85–106.
[21] J. Connolly: http://www.perplex.ethz.ch/perplex.
[22] W.B. Kamb, The thermodynamic theory of non-hydrostatically stressed solids, J. Geophys. Res. 66 (1961) 259–271.
[23] H.C. Hegelson, C.J. Bruton, Calculation of the chemical and thermodynamic consequences of differences between fluid and geostatic pressure in hydrothermal systems, Am. J. Sci. 283 (1983) 540–588.
[24] M.S. Paterson, D.L. Olgaard, Deformation tests to large shear strains in torsion, J. Struct. Geol. 22 (2000) 1341–1358.
[25] M. Pieri, Shear deformation of calcite rocks. Rheology and microfabric evolution of Carrara marble under dynamic recrystallization during torsion experiments, PhD thesis ETH-Zürich nr. 13220 (1999).
[26] A. Barnhoorn, Rheological and microstructural evolution of carbonate rocks during large strain torsion experiments, PhD thesis ETH-Zürich nr. 15309 (2003).
[27] N. Davis, Experimental deformation of natural and synthetic dolomite, Master thesis, Texas A&M University (2005).
[28] A.N. Walker, E.H. Rutter, K.H. Brodie, Experimental study of grain size sensitive flow of synthetic, hot pressed calcite rocks, in: R.J. Knipe, E.H. Rutter (Eds.), Deformation Mechanisms, Rheology and Tectonics, Geological Society Special Publication, vol. 54, 1990, pp. 259–284.
[29] T. Kenkmann, G. Dresen, Dislocation microstructure and phase distribution in a lower crustal shear zone—an example from the Ivrea zone, Italy, Int. J. Earth Sci. 91 (2002) 445–458.
[30] J. Tullis, R.A. Yund, Dynamic recrystallisation of feldspar: a mechanism for ductile shear zone formation, Geology 13 (1985) 238–241.
[31] M. Pieri, L. Burlini, K. Kunze, D. Olgaard, I. Stretton, Dynamic recrystallization of Carrara Marble during high temperature torsion experiments, J. Struct. Geol. 23 (2001) 1393–1413.
[32] A. Barnhoorn, M. Bystricky, L. Burlini, K. Kunze, The role of recrystallization on the deformation behaviour of calcite rocks: large strain torsion experiments on Carrara marble, J. Struct. Geol. 26 (2004) 885–903.
[33] S. Karato, M.S. Paterson, J. FitzGerald, Rheology of synthetic olivine aggregates: influence of grain size and water, J. Geophys. Res. 91 (1986) 8151–8176.
[34] E.H. Rutter, Experimental study of the influence of stress, temperature, and strain on the dynamic recrystallisation of Carrara marble, J. Geophys. Res. 100 (1995).
[35] J.H.P. De Bresser, C.J. Peach, J.P.J. Reijs, C.J. Spiers, On dynamic recrystallization during solid state flow; effects of stress and temperature, Geophys. Res. Lett. 25 (1998) 3457–3460.
[36] J.H.P. De Bresser, J. Ter Heege, C.J. Spiers, Grain size reduction by dynamic recrystallization: can it result in major rheological weakening? Int. J. Earth Sci. 90 (2001) 28–45.
[37] D.L. Olgaard, The role of second phase in localising deformation, in: R.J. Knipe, E.H. Rutter (Eds.), Deformation Mechanisms, Rheology and Tectonics, vol. 54, Geological Society of London, 1990, pp. 175–181.
[38] B. Evans, J. Renner, G. Hirth, A few remarks on the kinetics of static grain growth in rocks, Int. J. Earth Sci. 90 (2001) 88–103.
[39] M. Herweg, A. Berger, A. Ebert, Grain coarsening maps: a new tool to predict microfabric evolution of polymineralic rocks, Geology 33 (2005) 801–804.
[40] T.J.B. Holland, R. Powell, An internally consistent thermodynamic data set for phases of petrological interest, J. Metamorph. Geol. 16 (1998) 309–343.
[41] S.M. Schmid, M.S. Paterson, J.N. Boland, High temperature flow and dynamic crystallization in Carrara marble, Tectonophysics 65 (1980) 245–280.
[42] M.S. Paterson, C.W. Weaver, Deformation of polycrystalline MgO under pressure, J. Am. Ceram. Soc. 53 (1970) 463–471.
[43] M.R. Handy, Flow laws for rocks containing two non-linear viscous phases: a phenomenological approach, J. Struct. Geol. 16 (1994) 287–301.